COMMUNICATION

Check for updates

Enzymatic production of β-glucose 1,6-bisphosphate through manipulation of catalytic magnesium coordination†

Henry P. Wood, [ID] [a] Nicola J. Baxter,[a,b] F. Aaron Cruz-Navarrete, [ID] [a] Clare R. Trevitt,[a]
Andrea M. Hounslow[a] and Jonathan P. Waltho [ID] *[a,b]

Manipulation of enzyme behaviour represents a sustainable technology that can be harnessed to enhance the production of valuable metabolites and chemical precursors. β-Glucose 1,6-bisphosphate (βG16BP) is a native reaction intermediate in the catalytic cycle of β-phosphoglucomutase (βPGM) that has been proposed as a treatment for human congenital disorder of glycosylation involving phosphomannomutase 2. Strategies to date for the synthesis of βG16BP suffer from low yields or use chemicals and procedures with significant environmental impacts. Herein, we report the efficient enzymatic synthesis of anomer-specific βG16BP using the D170N variant of βPGM (βPGM$_{D170N}$), where the aspartate to asparagine substitution at residue 170 perturbs the coordination of a catalytic magnesium ion. Through combined use of NMR spectroscopy and kinetic assays, it is shown that the weakened affinity and reactivity of βPGM$_{D170N}$ towards βG16BP contributes to the pronounced retardation of the second step in the two-step catalytic cycle, which causes a marked accumulation of βG16BP, especially at elevated MgCl$_2$ concentrations. Purification, employing a simple environmentally considerate precipitation procedure requiring only a standard biochemical toolset, results in a βG16BP product with high purity and yield. Overall, this synthesis strategy illustrates how manipulation of the catalytic magnesium coordination of an enzyme can be utilised to generate large quantities of a valuable metabolite.

Enzyme engineering represents an emerging technology with the potential to deliver solutions to many sustainable development problems.[1,2] Biofuel production, plastic degradation and the clean generation of industrial reagents and precursors are three examples of areas where enzymes already make a signifi-

cant contribution.[3–6] Research that aims to foster a deeper understanding of enzyme catalysis is therefore of great interest. Phosphoryl transfer enzymes are at the forefront of research models for investigating the origins of enzyme catalysis because they exhibit some of the largest enzymatic rate enhancements known.[7,8] In addition, phosphate esters are often covalently incorporated into pharmaceutical products to improve bioavailability.[9,10] β-Phosphoglucomutase (βPGM; EC 5.4.2.6) has emerged as an archetypal enzyme in the study of phosphoryl transfer, and substantial progress has been made in understanding its mechanism of catalysis.[11–16] This magnesium-dependent enzyme from *Lactococcus lactis* (subspecies *lactis* IL1403) catalyses the isomerisation between β-glucose 1-phosphate (βG1P) and glucose 6-phosphate (G6P) *via* a β-glucose 1,6-phosphate (βG16BP) intermediate, which is released to solution before rebinding in the alternate orientation (Fig. 1).[11,17] The βG1P substrate of βPGM is commercially unavailable, but appropriate quantities for research have been produced enzymatically from maltose using a simple method involving maltose phosphorylase.[18] To initiate the catalytic cycle, βPGM requires priming with a phosphorylating agent to generate the active phospho-enzyme (βPGM^P, phosphorylated on residue D8) and βG16BP can perform this role *in vivo*. Since βG16BP is also commercially unavailable, alternative phosphorylating agents such as acetyl phosphate (AcP), fructose 1,6-bisphosphate (F16BP) and α-glucose 1,6-bisphosphate (αG16BP) have been used to generate βPGM^P *in vitro*, but these compounds are less effective and produce complicated kinetic behaviour.[12,19]

βG16BP has also been identified as a potential pharmacological chaperone for the management of a human congenital disorder of glycosylation involving phosphomannomutase 2.[20] Acting as a weakly binding competitive inhibitor, βG16BP is able to rescue the compromised activity of pathological variants of phosphomannomutase 2 by stabilising the protein fold. Therefore, further investigations of phosphomannomutase 2 and of βPGM are reliant on the availability of substantial quantities of βG16BP. Three strategies have been reported pre-

*[a]Krebs Institute for Biomolecular Research, Department of Molecular Biology and Biotechnology, The University of Sheffield, Sheffield, S10 2TN, UK.
E-mail: j.waltho@sheffield.ac.uk; Tel: +44 114 22717*
[b]Manchester Institute of Biotechnology and School of Chemistry, The University of Manchester, Manchester, M1 7DN, UK
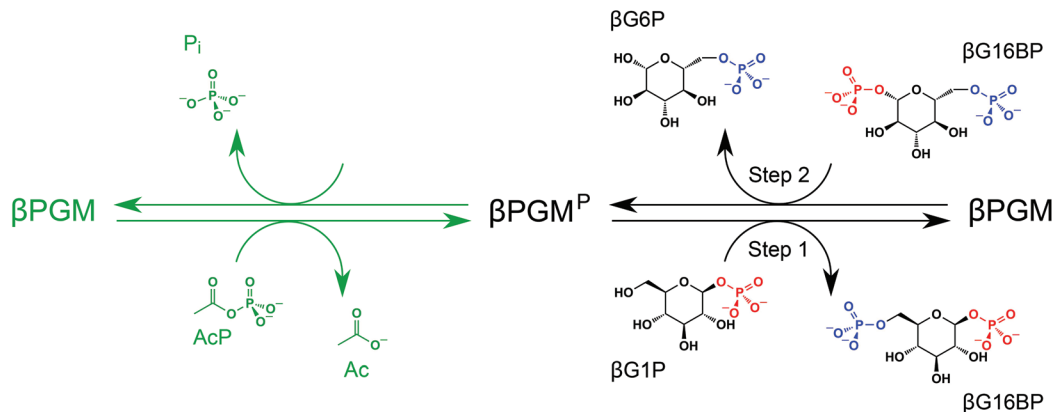†Electronic supplementary information (ESI) available. See DOI: 10.1039/d0gc03290e

Fig. 1 *In vitro* phosphorylation and catalytic cycle of βPGM. AcP phosphorylates βPGM generating βPGM^P (phosphorylated on residue D8) in a Mg^{2+}-independent reaction (green ink). In the Mg^{2+}-dependent catalytic cycle (black ink), Step 1 involves phosphoryl transfer from βPGM^P to the βG1P substrate forming the βG16BP intermediate, whereas Step 2 comprises phosphoryl transfer from βG16BP (bound in the alternate orientation) to βPGM forming the G6P product and regeneration of βPGM^P. In the phosphorylated glucosaccharide structures, 1-phosphate groups are coloured red and 6-phosphate groups are coloured blue. The black arrows denote the dominant direction of the corresponding reversible reactions. In the absence of the βG1P substrate, βPGM^P has a half-life of 30 s and hydrolyses readily to βPGM liberating inorganic phosphate (P$_i$).[12]

viously for the synthesis of βG16BP; however, each of these methods either delivers low yields or uses chemicals and procedures with significant environmental impacts. Firstly, the chemical synthesis of βG16BP from α-glucose involves an eight-step protocol, requiring considerable time and technical expertise, together with the use of harmful and environmentally hazardous reagents.[12] Low yields are obtained, since the β-anomer must be selected carefully on the basis of solubility from a racemic mixture of glucosaccharide products. Secondly, an enzymatic production method utilises a non-native reaction of phosphofructokinase to generate βG16BP from βG1P using adenosine triphosphate as the phosphoryl donor.[17,20] Purification of the product, though, cannot be achieved simply using precipitation procedures, since contaminating adenosine diphosphate co-precipitates with βG16BP,[21] and therefore ion-exchange HPLC purification is required. The use of HPLC columns is inherently damaging to the environment owing to the use of triethylammonium bicarbonate as a volatile buffer mobile phase, which during its production results in the release of large quantities of carbon dioxide.[22] Thirdly, an extraction method involves the removal of βG16BP from a variant of βPGM that co-purifies with a stoichiometric quantity of the molecule.[18] This method suffers from low yields, since it relies on very high recombinant βPGM production levels, and requires a week-long protein growth and purification procedure for each new batch of βG16BP. The limited availability of βG16BP therefore represents a significant barrier to the structural, kinetic and therapeutic investigations of phosphomutase enzymes. Herein, we describe a room-temperature, enzymatic method using the D170N variant of βPGM (βPGM$_{D170N}$) for the production of 100% anomer-specific βG16BP, which requires only micromolar quantities of enzyme and a simple environmentally considerate purification procedure that can be performed easily by a non-chemist over the course of two days. Through combined use of NMR spec-

troscopy and kinetic assays, it is shown that the weakened affinity and reactivity of βPGM$_{D170N}$ towards βG16BP contributes to the pronounced retardation of the second step in the two-step catalytic cycle, which causes a marked accumulation of βG16BP, especially at elevated MgCl$_2$ concentrations. More generally, this enzymatic synthesis strategy illustrates how manipulation of catalytic magnesium coordination can be utilised to generate large quantities of a valuable metabolite.

βPGM has two phosphoryl transfer steps in its catalytic cycle: Step 1 comprises phosphoryl transfer from βPGM^P to the βG1P substrate forming the βG16BP reaction intermediate, whereas Step 2 involves phosphoryl transfer from βG16BP to βPGM forming the G6P product and regeneration of βPGM^P (Fig. 1). When wild-type βPGM (βPGM$_{WT}$) is incubated in the presence of Mg^{2+} ions, with 20 mM AcP as the phosphorylating agent and 10 mM βG1P as a substrate, βG16BP generated in the catalytic cycle does not accumulate to detectable levels when monitored using ^{31}P NMR experiments.[18] Instead, βG16BP rebinds the enzyme with micromolar affinity in the alternate orientation, for the Step 2 reaction. Thus, the tight binding and high reactivity of βG16BP maintain a low steady state concentration, which precludes the harvesting of this species in useful quantities. The crystal structures of substrate-free βPGM$_{WT}$ (PDB: 6YDL[23]) and of the βPGM$_{WT}$^{P} analogue complex (βPGM$_{WT}$:BeF$_3$ complex, PDB: 2WFA[15]) indicate that the catalytic magnesium ion (Mg$_{cat}$) is coordinated through three enzyme atoms in the former and four phospho-enzyme atoms in the latter (Fig. 2). Therefore, the differential coordination of Mg$_{cat}$ provides an appropriate target with which to manipulate βPGM to shift the balance in the rate constants of Step 1 and Step 2 so that βG16BP will accumulate to a greater extent. Two potential strategies emerged where Step 2 could be retarded with respect to Step 1, which involved either performing the reactions of the catalytic cycle under Mg^{2+}-free conditions or perturbing Mg$_{cat}$ coordination through point
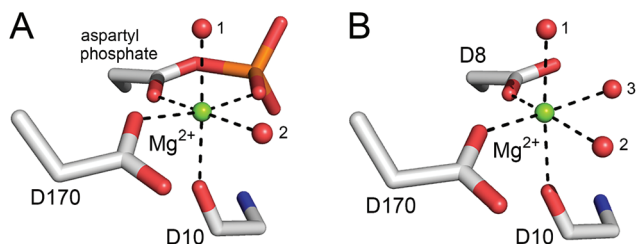
Fig. 2 Comparison of octahedral Mg_{cat} coordination in βPGM_{WT}^{P} (Step 1) and βPGM_{WT} (Step 2). (A) A model of βPGM_{WT}^{P} derived from the crystal structure of the βPGM_{WT}:BeF_3 complex (PDB: 2WFA[15]) showing Mg_{cat} coordination. The ligands comprise a carboxylate oxygen atom of residue D170, the carbonyl oxygen atom of residue D10 and two water molecules (indicated by numbers), together with the carboxylate oxygen atom and a phosphate oxygen atom of the D8 aspartyl phosphate moiety, creating bidentate coordination of Mg_{cat} in a six-membered ring of atoms. (B) The crystal structure of substrate-free βPGM_{WT} (PDB: 6YDL[23]) showing Mg_{cat} coordination. The ligands involve a carboxylate oxygen atom of residue D8, a carboxylate oxygen atom of residue D170, the carbonyl oxygen atom of residue D10 and three water molecules (indicated by numbers). Mg_{cat} is depicted as a green sphere, water molecules are illustrated as red spheres and metal ion coordination is shown as black dashes.

mutation to alter its binding properties. In either scenario, it was hypothesised that βPGM with a compromised Mg_{cat} site could be phosphorylated efficiently by reactive phosphorylating agents such as AcP, thereby generating βPGM^{P} and sub-

sequent reaction with $\beta G1P$ to produce $\beta G16BP$ in Step 1 (Fig. 1). In contrast, phosphorylation of βPGM by $\beta G16BP$ in Step 2 is less likely under these circumstances, which would lead to an accumulation of the reaction intermediate that could be harvested.

To explore whether AcP is able to phosphorylate Mg_{cat}-free βPGM_{WT}, ^{31}P NMR experiments were acquired to measure the change in AcP concentration over time in the presence and absence of 300 μM βPGM_{WT}. The addition of βPGM_{WT} resulted in a 25% increase in the rate of AcP hydrolysis (Fig. 3A), implying that βPGM_{WT}^{P} is generated and hydrolysed in the absence of Mg_{cat}. Consequently, the Step 1 reaction between Mg_{cat}-free βPGM_{WT} and 10 mM $\beta G1P$ in the presence of 50 mM AcP, together with the Step 2 production of G6P, was monitored using ^{31}P NMR time-course experiments. However, there was no detectable accumulation of $\beta G16BP$ (Fig. 4A–C) and the appearance of G6P product proceeded with a rate constant of 6.7×10^{-3} s^{-1}, which is 4 orders of magnitude smaller than the rate constant observed in the presence of 5 mM $MgCl_2$.[18] Hence, the observed enzymatic activity may simply arise due to the presence of very low levels of residual Mg^{2+} ions associated with the reagents. Taken together, these results indicate that both Mg_{cat}-bound βPGM_{WT}^{P} and Mg_{cat}-free βPGM_{WT}^{P} can be generated by AcP, but both the Step 1 and Step 2 phosphoryl transfer reactions are seriously impaired by the absence of Mg_{cat}.

Given the low rate of $\beta G16BP$ production in the absence of Mg^{2+} ions in the reaction buffer, a more subtle modification of
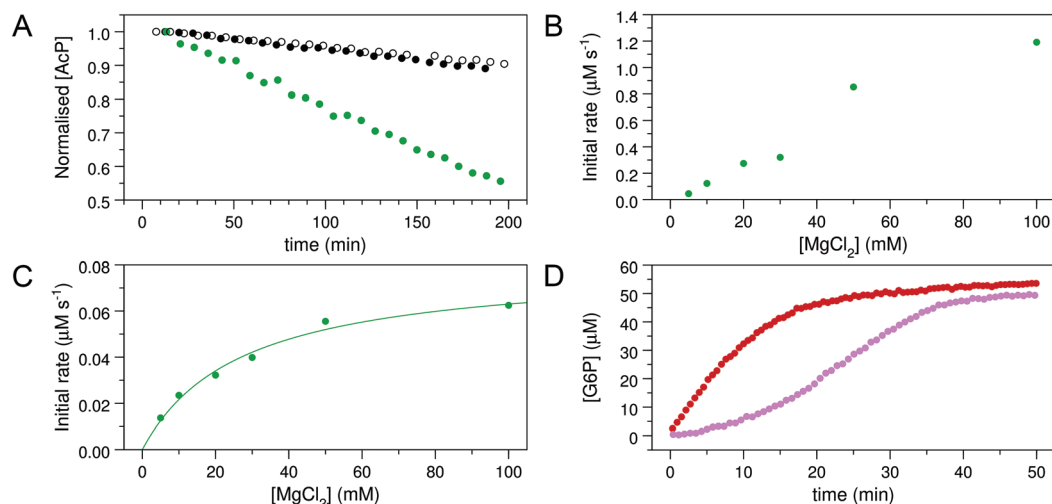

Fig. 3 Kinetic experiments involving βPGM_{WT} and βPGM_{D170N}. (A) Effect of βPGM_{WT} and βPGM_{D170N} on the hydrolysis of AcP monitored using ^{31}P NMR time-course experiments. AcP hydrolysis profiles were derived from normalised peak intensities obtained from reactions containing 50 mM AcP in 200 mM K$^+$ HEPES buffer (pH 7.2) without $MgCl_2$ (white circles) and separately in the presence of 300 μM βPGM_{WT} (black circles) or presence of 300 μM βPGM_{D170N} (green circles). (B and C) Activity of βPGM_{D170N} with increasing $MgCl_2$ concentration monitored using ^{31}P NMR time-course experiments. Samples contained 5 μM βPGM_{D170N} and 10 mM $\beta G1P$ in 200 mM K$^+$ HEPES buffer (pH 7.2), 10% ^2H_2O (v/v) and 1 mM TSP with increasing concentrations of $MgCl_2$ (5, 10, 20, 30, 50, 100 mM). The reactions were initiated by and timed from the addition of 20 mM AcP. Initial rate measurements for (B) the Step 1 production of $\beta G16BP$ and (C) the Step 2 production of G6P were obtained from linear least-squares fitting of normalised integral values of the ^{31}P resonances of $\beta G16BP$ and G6P present in the spectra. Subsequent fitting of the Step 2 initial rate values to eqn (1) using an in-house Python non-linear least squares fitting program yielded an apparent K_m (Mg^{2+}) = 27 ± 4 mM. (D) Kinetic profiles for the conversion of $\beta G1P$ to G6P by βPGM_{WT} monitored using a G6PDH coupled assay. Reactions were conducted in 200 mM K$^+$ HEPES buffer (pH 7.2) containing 5 mM $MgCl_2$, 1 mM NAD$^+$, 5 U mL^{-1} G6PDH, 50 μM $\beta G1P$ and 5 nM βPGM_{WT} with either 1 μM of the final $\beta G16BP$ product (red circles) or 8 mM AcP (pink circles) as the phosphorylating agent. For clarity, only half of the acquired data points have been included.
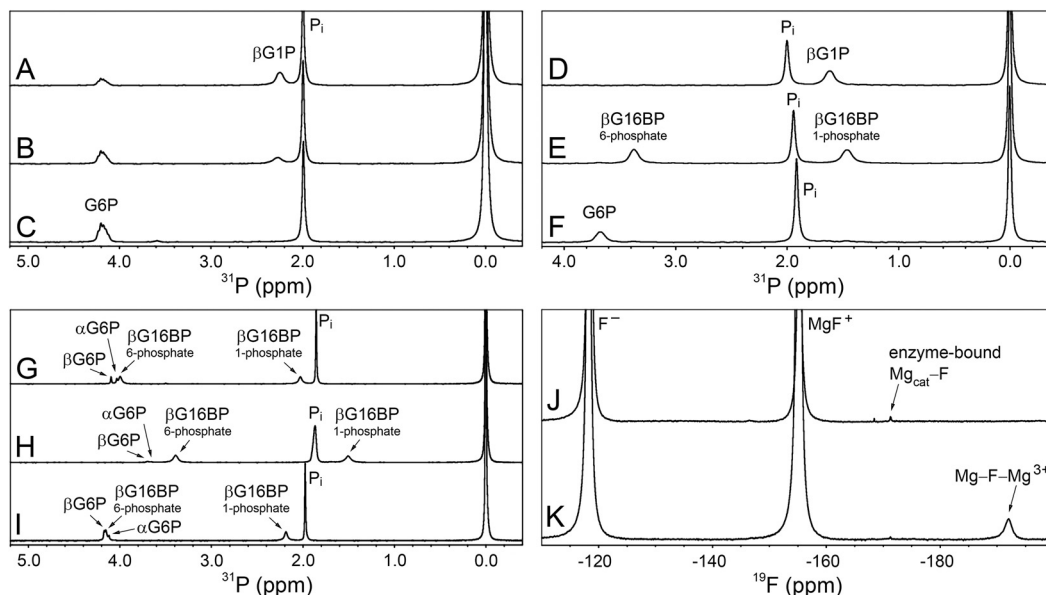
Fig. 4 ^{31}P and ^{19}F NMR experiments involving βPGM_{WT} and βPGM_{D170N}. (A–C) The βPGM_{WT}-catalysed conversion of $\beta G1P$ to G6P *via* $\beta G16BP$ in the absence of Mg^{2+} ions. (A) Reaction containing 300 μM βPGM_{WT} and 10 mM $\beta G1P$ in 200 mM K^+ HEPES buffer (pH 7.2) without $MgCl_2$, acquired 23 min after the addition of 50 mM AcP. (B) Reaction after 42 min showing the presence of $\beta G1P$ and G6P. (C) Reaction after 72 min showing complete conversion of $\beta G1P$ to G6P. (D–F) The βPGM_{D170N}-catalysed conversion of $\beta G1P$ to G6P, together with the accumulation of $\beta G16BP$. (D) Reaction containing 20 μM βPGM_{D170N} and 10 mM $\beta G1P$ in 200 mM K^+ HEPES buffer (pH 7.2) with 100 mM $MgCl_2$, prior to the addition of 20 mM AcP. (E) Reaction after 87 min showing the generation of $\beta G16BP$. (F) Reaction after 1179 min showing complete conversion of $\beta G1P$ to G6P. (G–I) The βPGM_{D170N}-catalysed conversion of $\beta G1P$ to G6P together with the accumulation of $\beta G16BP$ under variable ion concentrations. (G) Reaction containing 400 μM βPGM_{D170N} and 10 mM $\beta G1P$ in 200 mM K^+ HEPES buffer (pH 7.2) with 5 mM $MgCl_2$, 35 min after the addition of 20 mM AcP. (H) Reaction containing 400 μM βPGM_{D170N} and 10 mM $\beta G1P$ in 200 mM K^+ HEPES buffer (pH 7.2) with 100 mM $MgCl_2$, 19 min after the addition of 20 mM AcP. (I) Reaction containing 400 μM βPGM_{D170N} and 10 mM $\beta G1P$ in 200 mM K^+ HEPES buffer (pH 7.2) with 5 mM magnesium acetate and 200 mM NaCl, 36 min after the addition of 20 mM AcP. The peak at 1.9–2.0 ppm in panels A–I corresponds to inorganic phosphate (P_i), which is present in the stocks of both $\beta G1P$ and AcP. ^{31}P chemical shifts were referenced to external 1 M H_3PO_4 = 0.0 ppm, which was sealed inside a glass capillary and inserted into the sample NMR tubes. (J–K) ^{19}F NMR experiments involving βPGM_{D170N} acquired in 200 mM K^+ HEPES buffer (pH 7.2) at 5 °C. (J) A sample containing 0.5 mM βPGM_{D170N} with 5 mM $MgCl_2$, 10 mM NaF and 0.2 mM deferoxamine shows an enzyme-bound ^{19}F resonance (−171 ppm) that corresponds to a Mg_{cat}–F moiety. (K) A sample containing 0.5 mM βPGM_{D170N} with 100 mM $MgCl_2$, 10 mM NaF and 0.2 mM deferoxamine reveals that an increase in Cl^- ion concentration results in a decrease in the peak intensity of the Mg_{cat}–F moiety. Three free ^{19}F species are present in solution: Free F^- (−118 ppm), free MgF^+ (−155 ppm) and a free Mg–F–Mg^{3+} species (−192 ppm), which have been assigned based on the partitioning behaviour between discrete species as the $MgCl_2$ concentration is increased.

the enzyme Mg_{cat} site was engineered. In βPGM_{WT}, Mg_{cat} is co-ordinated octahedrally by a carboxylate oxygen atom of residue D8, a carboxylate oxygen atom of residue D170 and the carbonyl oxygen atom of residue D10, together with three water molecules. In βPGM_{WT}^P, one of the water molecules (water 3) is displaced by a phosphate oxygen atom of the D8 aspartyl phosphate moiety, creating bidentate coordination of Mg_{cat} in a six-membered ring of atoms (Fig. 2). Point mutations involving residue D8 have been reported to result in the complete loss of measurable catalytic activity.[19] Therefore, perturbation of Mg_{cat} was achieved through the generation of the D170N variant (βPGM_{D170N}), where the carboxamide group of residue N170 retains an oxygen atom with which to coordinate Mg_{cat}, but the sidechain is not charged. Accordingly, the reaction of βPGM_{D170N} with 10 mM $\beta G1P$ and 20 mM AcP in the presence of 100 mM $MgCl_2$ was monitored using ^{31}P NMR time-course experiments and, in contrast to βPGM_{WT}, the $\beta G16BP$ inter-mediate was observed to accumulate to a level comparable with the initial $\beta G1P$ concentration (Fig. 4D and E). The G6P product

was only generated to a measurable extent once the AcP concentration had reduced significantly (Fig. 4F). Hence, perturbation of Mg_{cat} in βPGM_{D170N} (in the presence of excess AcP) results in a substantial retardation of phosphorylation of βPGM_{D170N} by $\beta G16BP$ (Step 2) with respect to phosphorylation of $\beta G1P$ by βPGM_{D170N}^P (Step 1), therefore allowing $\beta G16BP$ to accumulate.

To investigate the source of the retardation of Step 2, glucose 6-phosphate dehydrogenase (G6PDH; EC 1.1.1.49) coupled assay experiments were conducted to assess the ability of βPGM_{D170N} to bind and convert the substrates of Step 2 ($\beta G16BP$) and Step 1 ($\beta G1P$). Initial rate measurements were recorded at increasing concentrations of $\beta G16BP$, which revealed that βPGM_{D170N} had an apparent K_m ($\beta G16BP$) = 150 ± 13 μM (Fig. S1A†). This value is 18-fold weaker than that measured for βPGM_{WT} (K_m ($\beta G16BP$) = 8.5 ± 0.3 μM (ref. 23)). Analogous experiments at increasing concentrations of $\beta G1P$ indicated that βPGM_{D170N} had an apparent K_m ($\beta G1P$) = 6.9 ± 1.0 μM, which is similar in magnitude to the K_m ($\beta G1P$) for βPGM_{WT} (K_m ($\beta G1P$) = 14.7 ± 0.5 μM (ref. 12)). These experi-

ments also demonstrated that a similar level of βG1P inhibition was operating in βPGM_{D170N} (apparent K_i (βG1P) = 1540 ± 170 µM) and βPGM_{WT} (K_i (βG1P) = 1510 ± 100 µM (ref. 23)) (Fig. S1B†). The K_m (Mg^{2+}) value for the overall reaction of βG1P to G6P was also measured for βPGM_{D170N} using increasing concentrations of $MgCl_2$ (Fig. S2†). These experiments resulted in an apparent K_m (Mg^{2+}) = 690 ± 110 µM, which is only 4-fold weaker than that determined for βPGM_{WT} using the same method (apparent K_m (Mg^{2+}) = 180 ± 40 µM). Overall, at 1 mM βG1P, 100 µM βG16BP and 5 mM $MgCl_2$ the observed rate constant for the overall reaction of βG1P to G6P catalysed by βPGM_{D170N} (k_{obs} = 3.0 × 10^{-3} s^{-1}) is 79 000-fold smaller than that for βPGM_{WT} (k_{obs} = 237 s^{-1}).

The observable accumulation of βG16BP in the ^{31}P NMR spectra of the βPGM_{D170N}-catalysed reaction (Fig. 4D–F) presented an opportunity to measure the effects of Mg^{2+} ion concentration on Step 1 and Step 2 independently within the same experiment (Fig. 1), although it should be noted that kinetic parameters obtained using ^{31}P NMR methods and the G6PDH coupled assay differ significantly due to the effects of the different conditions employed.[18,23] ^{31}P NMR time-course experiments were therefore conducted at increasing concentrations of $MgCl_2$ to measure simultaneously the initial rates of βG16BP production in Step 1 and G6P production in Step 2 (Fig. 3B and C). The initial rates of βG16BP production increased linearly with $MgCl_2$ concentration and so could not be fitted to a Michaelis–Menten equation over the concentration range 5–100 mM (Fig. 3B), indicating that the affinity of βPGM_{D170N} for Mg_{cat} in Step 1 is low. Extraction of the initial rates of G6P production in Step 2 resulted in an apparent K_m (Mg^{2+}) = 27 ± 4 mM (Fig. 3C). These observations therefore reveal that βG16BP accumulation can be greatly enhanced by using elevated concentrations of Mg^{2+} ions. For βPGM_{D170N} at 5 mM $MgCl_2$, the initial rate of Step 1 (k_{obs} = 9.0 × 10^{-3} s^{-1}) is only 3-fold faster than that of Step 2 (k_{obs} = 3.0 × 10^{-3} s^{-1}), while at 100 mM $MgCl_2$ Step 1 (k_{obs} = 0.24 s^{-1}) exceeds Step 2 (k_{obs} = 1.2 × 10^{-2} s^{-1}) by a factor of 20 (Fig. 3B, C and 4G, H). A control experiment employing elevated NaCl concentrations demonstrated that the increased initial rate of Step 1 at higher concentrations of $MgCl_2$ is not caused by Cl^- ions alone (Fig. 4I). Therefore, the Mg^{2+} ion concentration at which the production of βG16BP is performed has a strong bearing on its yield.

Taken together, this analysis demonstrates that the D170N point mutation causes a pronounced retardation of Step 2 together with a more modest change to Step 1. The reduced apparent K_m value of βPGM_{D170N} for βG16BP is in line with this behaviour. However, the substantially different apparent K_m (Mg^{2+}) values determined for Step 1 and Step 2 are not, which was surprising given the perturbation of the Mg_{cat} binding site in βPGM_{D170N}. One plausible explanation for these observations is that a Cl^- ion binds in the active site in substrate-free βPGM_{D170N} to mitigate the loss of the negative charge resulting from the D170N point mutation. The presence of a Cl^- ion at the Mg_{cat} binding site would rescue the binding of Mg_{cat} but hamper the binding of βG16BP and the approach of its phosphodianion to the carboxylate group of D8 in Step 2.

In contrast, AcP is able to generate $\beta PGM_{D170N}{}^P$ in a Mg_{cat}-independent manner (Fig. 1 and Fig. 3A) and the presence of the D8 aspartyl phosphate moiety will obviate the formation of the Mg_{cat}–Cl moiety.

To obtain evidence for a putative Mg_{cat}–halide moiety binding to substrate-free βPGM_{D170N}, 10 mM NaF was added to substrate-free βPGM_{D170N} containing 5 mM $MgCl_2$ and ^{19}F NMR experiments were recorded (Fig. 4J and K). A βPGM_{D170N}-bound ^{19}F species was observed with a chemical shift of −171 ppm, which corresponds to an analogous peak seen for substrate-free βPGM_{WT} acquired under similar conditions.[24] Elevation to 100 mM $MgCl_2$ did not result in increased saturation of Mg_{cat}, but instead reduced the ^{19}F peak integral to 80% of its size at 5 mM $MgCl_2$, suggesting that at higher concentrations, Cl^- ions are displacing the F^- ion bound at the Mg_{cat} site (Fig. 4J and K). In the experiment containing 100 mM $MgCl_2$, three free ^{19}F species are present in solution that are separated by chemical shift differences of exactly 37 ppm. Free F^- (−118 ppm) and free MgF^+ (−155 ppm) have been assigned previously,[24] whereas the peak resonating at −192 ppm is likely to be a free $Mg–F–Mg^{3+}$ species, based on the partitioning behaviour between discrete species as the $MgCl_2$ concentration is increased. Comparison of the chemical shifts of the βPGM_{D170N}-bound ^{19}F species with those of the three free species suggests that it is closer in identity to MgF^+. Therefore, the primary candidate for such an enzyme-bound species is a Mg_{cat}–F moiety, which in turn provides supporting evidence for the binding of a Mg_{cat}–Cl moiety to substrate-free βPGM_{D170N} that would consequently play a role in the retardation of Step 2 relative to Step 1.

The large-scale generation of βG16BP by the βPGM_{D170N}-catalysed reaction at high concentrations of $MgCl_2$ thus presented an opportunity for harvesting significant quantities of this valuable compound and so a robust production protocol was devised. Recombinant βPGM_{D170N} is overexpressed in high yields from *Escherichia coli* BL21(DE3) cells (>100 mg L^{-1}) using routine culture techniques and is readily purified using a two-step protocol involving ion-exchange chromatography followed by a size-exclusion chromatography step. βPGM_{D170N} can be stored at −20 °C for long periods and responds well to multiple freeze–thaw cycles, meaning that once purified, a batch of enzyme can be used for numerous βG16BP preparations. In order to characterise βPGM_{D170N} further, $^1H^{15}N$–TROSY NMR spectra were recorded using samples of ^{15}N-βPGM_{D170N} and ^{15}N-βPGM_{WT}. Comparison of the spectra revealed that βPGM_{D170N} has a similar solution behaviour and overall protein fold to βPGM_{WT} (Fig. S3†). The slow-exchange behaviour that arises in βPGM_{WT} from *cis*–*trans* proline isomerisation at the K145-P146 peptide bond is also observable in βPGM_{D170N}.[23] Notably, around 15 peaks are present for βPGM_{D170N} that are absent in the spectrum of βPGM_{WT}. These additional peaks indicate that a backbone conformational exchange process, occurring on the millisecond timescale in βPGM_{WT}, has been abolished in βPGM_{D170N}.[23]

To assess the stability of βPGM_{D170N} and to check for time-dependent reversion to βPGM_{WT} by deamidation,[25] a sample of βPGM_{D170N} was incubated at 25 °C for 48 h and both

[1]H[15]N–TROSY NMR spectra and ^{31}P NMR time-course experiments were acquired every 24 h. A comparison of [1]H[15]N–TROSY spectra recorded for βPGM$_{D170N}$ preincubated at 25 °C for 0 h and 48 h shows a near-identical correspondence of peaks indicating that the incubation process has a negligible effect on the integrity of βPGM$_{D170N}$ (Fig. S4A†). In comparisons of βPGM$_{D170N}$ and βPGM$_{WT}$ [1]H[15]N–TROSY spectra, the absence of observable βPGM$_{WT}$ peaks in the βPGM$_{D170N}$ spectra indicates that reversion of βPGM$_{D170N}$ to βPGM$_{WT}$ through deamidation is not a process that occurs readily under these sample conditions (Fig. S4B and C†). Analysis of the ^{31}P NMR time-course experiments for the equilibration of 10 mM βG1P with G6P catalysed by βPGM$_{D170N}$ (preincubated at 25 °C for 0 h, 24 h and 48 h) demonstrates a consistent behaviour of βG16BP production followed by conversion to G6P as product with no change in k_{obs}, further confirming the stability of βPGM$_{D170N}$ (Fig. S5A†).

To mimic the effect of βPGM$_{D170N}$ reversion to βPGM$_{WT}$ through deamidation, a control ^{31}P NMR time-course experiment was also conducted using a sample of βPGM$_{D170N}$ that had been spiked with 0.1% βPGM$_{WT}$ (Fig. S5B†). The kinetic profile shows an initial burst of G6P production by βPGM$_{WT}$ together with a decrease in the ratio of the βG16BP concentration at its maximum (βG16BP$_{max}$) to the concentration of G6P at its maximum (G6P$_{max}$). The ^{31}P NMR time-course experiments testing βPGM$_{D170N}$ stability revealed no burst of G6P production nor any change in either k_{obs} or the βG16BP$_{max}$:G6P$_{max}$ ratio. Together, these results indicate that βPGM$_{D170N}$ does not undergo detectable deamidation to βPGM$_{WT}$ and is stable at 25 °C over a 48-hour time frame.

^{31}P NMR time-course experiments were used to monitor the βPGM$_{D170N}$-catalysed conversion of βG1P to G6P to determine the optimal point at which to harvest βG16BP. In a representative reaction (see Materials and Methods) the βG16BP concentration reached a maximum after 265 min at 25 °C. Following quenching of the reaction at this point, and removal of βPGM$_{D170N}$, the solution was found to contain βG16BP alongside contaminants that included significant amounts of βG1P, G6P and inorganic phosphate (P$_i$), in a ratio of 1 : 0.07 : 0.2 : 3.9, respectively. As substrates of βPGM, these phosphorylated impurities are undesirable, therefore the solution was subjected to a barium salt precipitation and ion-exchange protocol to obtain the sodium salt of βG16BP with high purity. Barium salts of phosphate species are relatively insoluble,[26] and the difference in relative solubility of the βG16BP barium salt compared with those of βG1P and G6P was exploited to enable purification.[27–29]

To confirm the identity and assess the purity of the final βG16BP product, a sample of the fine powder was analysed using ^{1}H, ^{13}C and ^{31}P NMR experiments (Fig. 5A–D). The identity of the resulting compound was established to be βG16BP by comparison of ^{1}H and ^{13}C chemical shifts with previously reported values.[12] Glucose and maltose contaminants were identified in the sample using ^{1}H chemical shifts and scalar coupling constants (BMRB: bmse000015, BMRB: bmse000017). Based on integral values of the anomeric proton signals and of the phosphorus signals in quantitative ^{1}H and ^{31}P NMR spectra, the βG16BP concentration was determined to be 67 mM, which represented 98% of the total phosphorylated glucosaccharide components and 72% of the total glucosac-
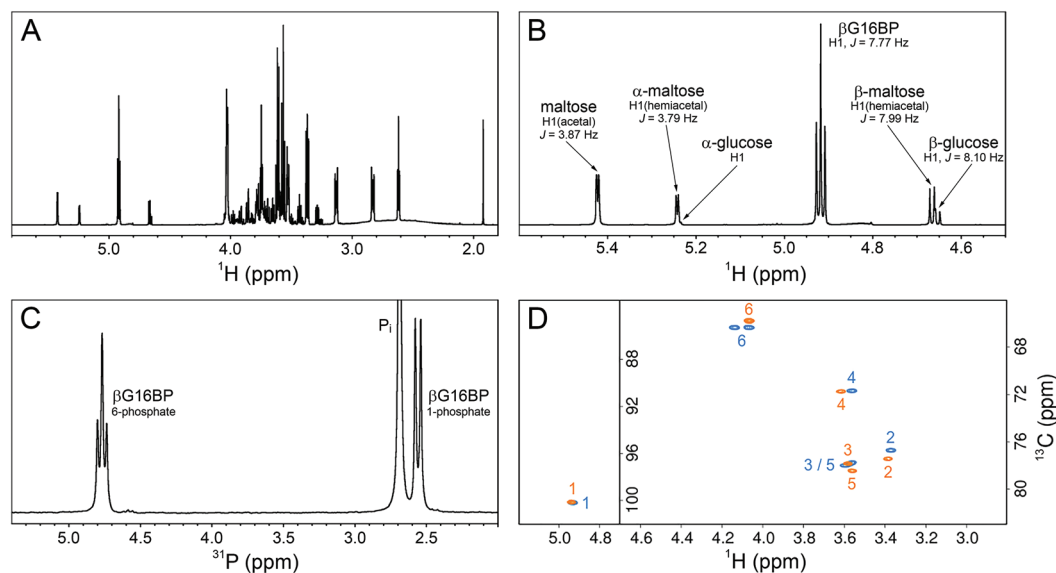

Fig. 5 NMR experiments recorded on a sample of the final βG16BP product, purified following its production by βPGM$_{D170N}$ and prepared in 100% [2]H$_2$O. (A) ^{1}H spectrum showing βG16BP and other glucosaccharide species present in the sample. (B) A region of the ^{1}H spectrum showing the anomeric proton glucosaccharide signals, together with their assignments. (C) ^{31}P spectrum showing the two phosphorus signals of βG16BP (6-phosphate, 4.76 ppm (triplet) and 1-phosphate, 2.55 ppm (doublet)) and the signal corresponding to inorganic phosphate (P$_i$, 2.70 ppm (singlet), truncated for clarity). (D) Natural abundance [1]H[13]C–HSQC spectra comparing the final βG16BP product (orange) with chemically synthesised βG16BP (blue).[12] Peaks are labelled with carbon ring atom assignments.

charide components present in the final sample. βG1P, G6P and glucose comprised <1%, 1% and 3%, respectively, of the total glucosaccharide content. Maltose was present at a greater concentration in the sample (24%), but as a bystander in the reactions of βPGM, and not known to bind to phosphomanno-mutase 2, this contamination is unlikely to be problematic for users. P_i was also present at a concentration 2.9-fold higher than that of βG16BP. The glucose, maltose and P_i components, which were carried through into the final βG16BP product, are contaminants derived from the enzymatic synthesis of βG1P and would otherwise not be present if a purer source of βG1P were used. Residual HEPES buffer and acetate were also present as minor contaminants. The final yield for the βPGM$_{D170N}$-catalysed conversion of βG1P to βG16BP was 33.6% and the yield for the overall conversion of maltose to βG16BP was 7.7%. Since the equilibrium for the enzymatic conversion of maltose to βG1P lies in favour of maltose, conducting the reactions for the maltose phosphorylase synthesis of βG1P and the βPGM$_{D170N}$ synthesis of βG16BP in a one-pot system is likely to lead to higher βG16BP yields. The removal of βG1P by βPGM$_{D170N}$ would drive the maltose reaction to produce more βG1P, which in turn would result in a greater overall yield of βG16BP. This approach has been demonstrated previously for the protocol involving maltose phosphorylase and phos-phofructokinase.[17] To demonstrate the biochemical effective-ness of the final βG16BP product at activating βPGM$_{WT}$, a kinetic experiment was conducted using the G6PDH coupled assay. βPGM$_{WT}$ was mixed with the βG1P substrate and acti-vated using either 1 μM βG16BP (produced using βPGM$_{D170N}$) or 8 mM AcP as the phosphorylating agent. The kinetic profile obtained was linear for the βG16BP-containing reaction, but exhibited a lag phase when AcP was used (Fig. 3D). As βG16BP is the only phosphorylating agent known to induce linear initial kinetics in βPGM,[23] this experiment provided a clear demonstration of the activity of the final βG16BP product.

Conclusions

The successful manipulation of βPGM behaviour to facilitate βG16BP production is a demonstration of how detailed struc-tural and mechanistic knowledge of an enzyme can lead to novel engineering strategies. Specifically, the modification of the metal binding site of the enzyme dramatically increases the steady state concentration of its reactive intermediate. This highlights the transformative potential that enzymes have within chemical industries and vindicates the intensive study of these useful biomolecules.

Materials and methods

Reagents

Unless stated otherwise, reagents were purchased from Sigma-Aldrich, Fischer Scientific, Alfa Aesar and VWR. Isotopically enriched $^{15}NH_4Cl$ was purchased from CortecNet.

Gene sequence for βPGM$_{D170N}$

CATATGTTTAAAGCAGTATTGTTTGATTTAGATGGTGTAATTA
CAGATACCGCAGAGTATCATTTTAGAGCTTGGAAAGCTTTGG
CTGAAGAAATTGGCATTAATGGTGTTGACCGCCAATTTAATG
AGCAATTAAAAGGGGTCTCACGAGAAGACTCGCTTCAGAAAA
TTCTAGATTTAGCTGATAAAAAAGTATCAGCTGAGGAATTTAA
AGAACTTGCTAAGAGAAAAAATGATAACTATGTGAAAATGATT
CAGGATGTGTCGCCAGCCGATGTCTATCCTGGAATTTTACAAT
TACTCAAAGATTTACGTTCAAATAAAATCAAAATTGCTTTAGCG
TCGGCTTCTAAGAATGGTCCATTTTTATTAGAGAGAATGAATTT
AACTGGATATTTTGATGCAATTGCTGATCCGGCTGAAGTTGCAG
CATCAAAACCAGCACCAGATATTTTTATTGCAGCAGCACATGCA
GTGGGTGTTGCCCCCTCTGAATCAATTGGGTTAGAGAATTCTCA
AGCTGGAATTCAAGCCATCAAAGATTCAGGGGCTTTACCAATTG
GTGTAGGGCGCCCAGAAGATTTGGGAGATGATATCGTCATTGT
GCCTGATACTTCACACTATACATTAGAATTTTTGAAAGAAGTTTG
GCTTCAAAAGCAAAAATAACTCGAG.

βPGM expression and purification

The βPGM$_{D170N}$ gene sequence was created by modifying the *pgmB* gene (encoding the βPGM$_{WT}$ enzyme) from *Lactococcus lactis* (subspecies *lactis* IL1403) (NCBI: 1114041). The βPGM$_{D170N}$ gene was generated and cloned by GenScript into a pET22b(+) vector. The βPGM$_{WT}$ and βPGM$_{D170N}$ plasmids were transformed into *Escherichia coli* BL21(DE3) cells and grown using ^{15}N isotopically enriched M9 minimal media.[30] Cells were grown to an OD$_{600}$ of 0.6 at 37 °C and over-expression was induced with 0.5 mM (final concentration) isopropyl β-D-1-thiogalactopyranoside (IPTG) before a 16-hour incubation at 25 °C and centrifugation (Sigma Model 3-15; 9000 rpm for 10 min) to harvest the cells. The βPGM$_{WT}$ and βPGM$_{D170N}$ proteins were purified using the following proto-col. The cell pellet was resuspended in ice-cold standard buffer (50 mM K$^+$ HEPES buffer (pH 7.2), 5 mM MgCl$_2$, 2 mM NaN$_3$, 1 mM EDTA) containing a cOmplete protease inhibitor cocktail. The cell suspension was sonicated on ice for 6 × 20 s pulses separated by 60 s intervals. The cell lysate was separ-ated from the insoluble cell debris using centrifugation (Beckman Coulter Avanti centrifuge, Rotor: JA-25-50) at 20 000 rpm for 30 min at 4 °C. The soluble fraction was loaded onto a DEAE-Sepharose anion-exchange column con-nected to an ÄKTA Prime purification system, which had been washed previously with 1 M NaOH and 6 M guanidi-nium chloride and equilibrated with 5 column volumes of standard buffer. Bound proteins were eluted using a gradient of 0 to 50% standard buffer supplemented with 1 M NaCl over 300 mL. Fractions containing βPGM were identified using SDS-PAGE and were concentrated to a 5–10 mL volume using centrifugation in a Vivaspin (10 kDa molecular weight cut off; Sartorius) at 4500 rpm and 4 °C (Thermo Scientific Heraeus Labofuge 400 R). The concentrated protein sample was loaded onto a pre-packed Hiload 26/600 Superdex 75 size-exclusion column connected to an ÄKTA Prime purification system, which had been washed previously with degassed 1 M

NaOH and equilibrated with 3 column volumes of degassed standard buffer supplemented with 1 M NaCl. Following elution, the fractions containing βPGM were checked for purity and were pooled and buffer-exchanged into standard buffer for βPGM$_{WT}$ and standard buffer containing 50 mM MgCl$_2$ for βPGM$_{D170N}$. Mg$_{cat}$-free βPGM$_{WT}$ and Mg$_{cat}$-free βPGM$_{D170N}$ were prepared by buffer-exchanging into standard buffer without MgCl$_2$. The final protein samples were concentrated using a Vivaspin (10 kDa molecular weight cut off; Sartorius) to a 1 mM concentration, as measured by Nanodrop One^C (Thermo Scientific) (βPGM molecular weight = 24.2 kDa, ε_{280} = 19 940 M^{-1} cm^{-1}), and were stored at −20 °C.

NMR spectroscopy

All NMR spectra were acquired at 298 K, unless stated otherwise. ^{31}P NMR time-course experiments were acquired using a Bruker 500 MHz Avance II spectrometer (operating at 202.456 MHz for ^{31}P) equipped with a 5 mm room-temperature broadband probe and running TopSpin version 3.5. One-dimensional experiments consisting of 256 transients were recorded with a recycle delay of 1 s with proton-phosphorus decoupling and took 479.4 s to acquire. Where stated, experiments were acquired without phosphorus decoupling and took 370.4 s to record. For the AcP hydrolysis experiments, no proton-phosphorus decoupling was used and samples contained 50 mM AcP in 200 mM K$^+$ HEPES buffer (pH 7.2), 10% ^{2}H$_2$O (v/v) and 1 mM trimethylsilyl propionate (TSP) without MgCl$_2$, together with either 300 μM βPGM$_{WT}$ or 300 μM βPGM$_{D170N}$. For the reactions involving the βPGM-catalysed conversion of βG1P to G6P, samples contained: 300 μM βPGM$_{WT}$, 10 mM βG1P and 50 mM AcP in 200 mM K$^+$ HEPES buffer (pH 7.2), 10% ^{2}H$_2$O (v/v) and 1 mM TSP without MgCl$_2$ and with no proton-phosphorus decoupling used; 20 μM βPGM$_{D170N}$, 10 mM βG1P and 20 mM AcP in 200 mM K$^+$ HEPES buffer (pH 7.2), 10% ^{2}H$_2$O (v/v) with 100 mM MgCl$_2$ and with no proton-phosphorus decoupling used; 400 μM βPGM$_{D170N}$, 10 mM βG1P and 20 mM AcP in 200 mM K$^+$ HEPES buffer (pH 7.2), 10% ^{2}H$_2$O (v/v) and 1 mM TSP with 5 mM MgCl$_2$; 400 μM βPGM$_{D170N}$, 10 mM βG1P and 20 mM AcP in 200 mM K$^+$ HEPES buffer (pH 7.2), 10% ^{2}H$_2$O (v/v) and 1 mM TSP with 100 mM MgCl$_2$; 400 μM βPGM$_{D170N}$, 10 mM βG1P and 20 mM AcP in 200 mM K$^+$ HEPES buffer (pH 7.2), 10% ^{2}H$_2$O (v/v) and 1 mM TSP with 5 mM magnesium acetate and 200 mM NaCl. For the βPGM$_{D170N}$ stability measurements, samples contained 200 μM βPGM$_{D170N}$ (preincubated at 25 °C either for 0 h, 24 h or 48 h), 10 mM βG1P and 20 mM AcP in 200 mM K$^+$ HEPES buffer (pH 7.2), 10% ^{2}H$_2$O (v/v) and 1 mM TSP with 100 mM MgCl$_2$. For the experiment representative of 0.1% reversion of βPGM$_{D170N}$ to βPGM$_{WT}$ through deamidation, the sample contained 200 μM βPGM$_{D170N}$ and 200 nM βPGM$_{WT}$, 10 mM βG1P and 20 mM AcP in 200 mM K$^+$ HEPES buffer (pH 7.2), 10% ^{2}H$_2$O (v/v) and 1 mM TSP with 100 mM MgCl$_2$. To measure apparent K_m (Mg^{2+}) values for the Step 1 production of βG16BP and the Step 2 production of G6P, samples contained 5 μM βPGM$_{D170N}$, 10 mM βG1P and 20 mM AcP in 200 mM K$^+$

HEPES buffer (pH 7.2), 10% ^{2}H$_2$O (v/v) and 1 mM TSP with increasing concentrations of MgCl$_2$ (5, 10, 20, 30, 50, 100 mM). ^{19}F experiments were recorded at 278 K using a Bruker 500 MHz Avance III spectrometer (operating at 470.59 MHz for ^{19}F) equipped with a 5 mm QCI-F cryoprobe and z-axis gradients running TopSpin version 3.5. One-dimensional experiments consisting of 16384 transients were recorded with a recycle delay of 1 s and took 352 min to acquire. Samples of 0.5 mM βPGM$_{D170N}$ were prepared in 200 mM K$^+$ HEPES buffer (pH 7.2) containing 5 mM or 100 mM MgCl$_2$, 10 mM NaF, 0.2 mM deferoxamine, 10% ^{2}H$_2$O (v/v) and 1 mM TSP. ^{1}H^{15}N–TROSY NMR spectra were recorded for βPGM$_{WT}$ using a Bruker 500 MHz Avance III spectrometer equipped with a 5 mm QCI-F cryoprobe and z-axis gradients running TopSpin version 3.5. The sample contained 1 mM ^{15}N-βPGM$_{WT}$ in 50 mM K$^+$ HEPES buffer (pH 7.2) with 5 mM MgCl$_2$, 2 mM NaN$_3$, 10% (v/v) ^{2}H$_2$O and 1 mM TSP. ^{1}H^{15}N–TROSY NMR spectra were recorded for βPGM$_{D170N}$ using a Bruker 800 MHz Neo spectrometer equipped with a 5 mm TCI cryoprobe and z-axis gradients running TopSpin version 4.0. The sample contained 0.5 mM ^{15}N-βPGM$_{D170N}$ (preincubated at 25 °C either for 0 h, 24 h or 48 h) in 50 mM K$^+$ HEPES buffer (pH 7.2) with 5 mM MgCl$_2$, 2 mM NaN$_3$, 10% (v/v) ^{2}H$_2$O and 1 mM TSP. ^{1}H^{15}N–TROSY experiments were acquired with 16 transients with 256 increments and spectral widths of 32 or 36 ppm centred at 120 ppm or 118 ppm in the indirect ^{15}N dimension. For the final βG16BP product prepared in 100% ^{2}H$_2$O containing 1 mM TSP, ^{1}H and natural abundance ^{1}H^{13}C–HSQC experiments were recorded using standard Bruker pulse sequences on an 800 MHz Bruker Neo spectrometer with a 5 mm TCI cryoprobe equipped with z-axis gradients and running TopSpin version 4.0. ^{31}P experiments were also recorded for this sample, as described above. ^{1}H and ^{13}C chemical shifts were referenced to TSP resonating at 0.0 ppm. ^{31}P experiments were either referenced to 1 M H$_3$PO$_4$ resonating at 0.0 ppm, sealed inside a glass capillary and inserted into the sample NMR tube or were referenced indirectly to TSP using the gyromagnetic ratios of the ^{1}H and ^{31}P nuclei. ^{19}F experiments were referenced indirectly to TSP using the gyromagnetic ratios of the ^{1}H and ^{19}F nuclei. NMR data were processed with baseline correction and Lorentzian apodisation using either FELIX (Felix NMR, Inc.) or TopSpin version 4.0 (Bruker). Quantitative NMR experiments were performed using a recycle delay of 60 s. To measure apparent K_m (Mg^{2+}) values from ^{31}P NMR time-course experiments, the initial rate for the Step 1 production of βG16BP and the Step 2 production of G6P was obtained using an in-house Python linear least-squares fitting program. The initial rates were subsequently fitted to eqn (1) using an in-house Python non-linear least-squares fitting program, which uses bootstrap error estimation.

$$v_0 = \frac{V_{max}[A]}{K_{m(app)} + [A]} \tag{1}$$

where v_0 represents the initial rate of reaction, A represents the activator being tested, V_{max} represents the apparent maximal

rate, $K_{m(app)}$ represents the apparent Michaelis constant for activation of the enzyme by A.

Kinetic assays

Kinetic assays for βPGM_{WT} and βPGM_{D170N} were conducted using a G6PDH coupled assay. Here, the G6P product of βPGM activity is oxidised to 6-phosphogluconolactone by G6PDH, while the concomitant reduction of NAD^+ to NADH is monitored by measuring changes in absorbance at 340 nm (ε_{340} = 6220 M^{-1} cm^{-1}). Reactions were run at 25 °C using a FLUOstar OMEGA microplate reader (BMG Labtech). To measure the $MgCl_2$ dependence of the βPGM_{WT}- and βPGM_{D170N}-catalysed conversion of $\beta G1P$ to G6P, reactions (160 μL) were conducted in 200 mM K^+ HEPES buffer (pH 7.2) containing different concentrations of $MgCl_2$ (0, 0.1, 0.3, 0.6, 1.0, 1.5, 2.5, 5, 10, 20, 50 and 100 mM), 1 mM NAD^+, 5 U mL^{-1} G6PDH, 1 mM $\beta G1P$ and either 1 nM βPGM_{WT} with 100 μM $\beta G16BP$, or 10 μM βPGM_{D170N} with 1250 μM $\beta G16BP$. Initial rates of the reactions were obtained using an in-house Python linear least-squares fitting program. Initial rates were subsequently fitted to eqn (2) using an in-house Python non-linear least-squares fitting program, which uses bootstrap error estimation.

$$v_0 = \frac{V_{max}[A]}{K_{m(app)} + [A]\left(1 + \dfrac{[A]}{K_i}\right)} \tag{2}$$

where v_0 represents the initial rate of reaction, A represents the activator being tested, V_{max} represents the apparent maximal rate, $K_{m(app)}$ represents the apparent Michaelis constant for activation of the enzyme by A and K_i represents the apparent inhibition constant of the enzyme for A. To measure the apparent K_m ($\beta G16BP$) of βPGM_{D170N}, reactions (160 μL) were conducted in 200 mM K^+ HEPES buffer (pH 7.2) with 5 mM $MgCl_2$, 1 mM NAD^+, 5 U mL^{-1} G6PDH, 10 μM βPGM_{D170N} and 1 mM $\beta G1P$, and were initiated using increasing concentrations of $\beta G16BP$ (10, 25, 50, 100, 150, 250, 350, 750, 1000, 1500, 2500 μM). Initial rates of G6P production were obtained using a linear least-squares fitting routine and these rates were subsequently fitted to eqn (1) using an in-house Python non-linear least squares fitting program. To measure the dependence of initial reaction velocity for βPGM_{D170N} on $\beta G1P$ concentration, reactions (160 μL) were conducted in 200 mM K^+ HEPES buffer (pH 7.2) with 5 mM $MgCl_2$, 1 mM NAD^+, 5 U mL^{-1} G6PDH, 10 μM βPGM_{D170N} and increasing concentrations of $\beta G1P$ (50, 100, 200, 300, 500, 700, 1000, 1500, 2000, 3000, 5000 μM) and were initiated using 250 μM $\beta G16BP$. Initial rates of G6P production were obtained using a linear least-squares fitting routine and these rates were subsequently fitted to eqn (2) to derive values for apparent K_m ($\beta G1P$) and apparent K_i ($\beta G1P$). To measure the effect of different phosphorylating agents on the βPGM_{WT}-catalysed conversion of $\beta G1P$ to G6P, reactions (160 μL) were conducted in 200 mM K^+ HEPES buffer (pH 7.2) with 5 mM $MgCl_2$, 1 mM NAD^+, 5 U mL^{-1} G6PDH, 5 nM βPGM_{WT}, 50 μM $\beta G1P$ with either 1 μM of the final $\beta G16BP$ product or 8 mM AcP as the phosphorylating agent. Blank absorbance measurements were obtained using solutions identical to the reaction mixtures, but without the addition of βPGM.

βG1P preparation

$\beta G1P$ was prepared enzymatically from maltose using maltose phosphorylase (EC 2.4.1.8). A solution of 611 mM maltose was incubated overnight with 1.2 U mL^{-1} maltose phosphorylase in 0.5 M sodium phosphate buffer (pH 7.0) at 30 °C. The production of $\beta G1P$ was confirmed using ^{31}P NMR spectroscopy. Maltose phosphorylase (molecular weight = 90 kDa) was removed from the solution by centrifugation using a Vivaspin (5 kDa molecular weight cut off; Sartorius). The concentration of $\beta G1P$ in the flow-through was measured to be 149 mM using quantitative ^{31}P NMR experiments in which a known amount of G6P had been added to a sample of the $\beta G1P$ product, along with 10% ^2H_2O (v/v) and 1 mM TSP. This concentration represents a yield of 24%. The $\beta G1P$ product was contaminated with glucose, maltose and P_i (estimated concentrations were 150 mM, 850 mM and 350 mM, respectively), and was not purified further since these compounds are bystanders in the reaction catalysed by βPGM.

βG16BP production and purification

A 15 mL reaction was prepared containing 20 μM βPGM_{D170N} in 200 mM K^+ HEPES buffer together with 100 mM $MgCl_2$, 2 mM NaN_3, 20 mM $\beta G1P$ and was initiated with 40 mM AcP. The concentration of $\beta G16BP$ reached a maximum after 265 min, whereupon the reaction was quenched by heat-denaturation of βPGM_{D170N} at 90 °C for 10 min. Precipitated enzyme was pelleted using centrifugation (Sigma Model 3-15) and the $\beta G16BP$-rich supernatant was collected and filtered with a Vivaspin (5 kDa molecular weight cut off; Sartorius) using a benchtop centrifuge (Thermo Scientific Heraeus Labofuge 400 R). The resulting enzyme-free solution was passed through a 20 × 10 mm column packed with IR120 (H^+) ion-exchange resin, which had been washed with 15 mL of milliQ water. This step acidified the solution, which was then neutralised using 0.2 M barium hydroxide solution, resulting in significant precipitation. The solution was kept on ice during neutralisation to increase the solubility of the mono-phosphorylated glucosaccharide barium salts.[31] Fractions obtained along the course of the barium salt formation were analysed using ^{31}P NMR experiments, which indicated that the $\beta G16BP$ barium salt was contained mainly in the precipitate, and that the $\beta G1P$ and G6P barium salts remained in solution. The precipitate was pelleted using centrifugation at 4 °C (4500 rpm, Thermo Scientific Heraeus Labofuge 400 R) and the supernatant was discarded. To convert the $\beta G16BP$ barium salt to the more soluble sodium salt the pellet was resolubilised in a large volume (~1 L) of cold milliQ water and passed through a 20 × 10 mm column packed with IR120 (Na^+) ion-exchange resin. The flow-through was then frozen at −80 °C and lyophilised to leave a fine powder as the final $\beta G16BP$ product.

Conflicts of interest

There are no conflicts to declare.

Acknowledgements

References

1 P.-S. Huang, S. E. Boyken and D. Baker, The coming of age of *de novo* protein design, *Nature*, 2016, **357**, 320–327.

2 K. Chen and F. H. Arnold, Engineering new catalytic activities in enzymes, *Nat. Catal.*, 2020, **3**, 203–213.

3 D. N. Bolon and S. L. Mayo, Enzyme-like proteins by computational design, *Proc. Natl. Acad. Sci. U. S. A.*, 2001, **98**, 14274–14279.

4 F. Wen, N. U. Nair and H. Zhao, Protein engineering in designing tailored enzymes and microorganisms for biofuels production, *Curr. Opin. Biotechnol.*, 2009, **20**, 412–419.

5 A. Zanghellini, *De novo* computational enzyme design, *Curr. Opin. Biotechnol.*, 2014, **29**, 132–138.

6 S. Yoshida, K. Hiraga, T. Takehana, I. Taniguchi, H. Yamaji, Y. Maeda, K. Toyohara, K. Miyamoto, Y. Kimura and K. Oda, A bacterium that degrades and assimilates poly(ethylene terephthalate), *Science*, 2016, **351**, 1196–1199.

7 R. Wolfenden and M. J. Snider, The depth of chemical time and the power of enzymes as catalysts, *Acc. Chem. Res.*, 2001, **34**, 938–945.

8 C. Lad, N. H. Williams and R. Wolfenden, The rate of hydrolysis of phosphomonoester dianions and the exceptional catalytic proficiencies of protein and inositol phosphatases, *Proc. Natl. Acad. Sci. U. S. A.*, 2003, **100**, 5607–5610.

9 S. Jones and D. Selitsianos, A simple and effective method for phosphoryl transfer using TiCl$_4$ catalysis, *Org. Lett.*, 2002, **4**, 3671–3673.

10 S. Jones, D. Selitsianos, K. J. Thompson and S. M. Toms, An improved method for Lewis acid catalyzed phosphoryl transfer with Ti(*t*-BuO)$_4$, *J. Org. Chem.*, 2003, **68**, 5211–5216.

11 J. Dai, L. Finci, C. Zhang, S. Lahiri, G. Zhang, E. Peisach, K. N. Allen and D. Dunaway-Mariano, Analysis of the structural determinants underlying discrimination between substrate and solvent in β-phosphoglucomutase catalysis, *Biochemistry*, 2009, **48**, 1984–1995.

12 M. Goličnik, L. F. Olguin, G. Feng, N. J. Baxter, J. P. Waltho, N. H. Williams and F. Hollfelder, Kinetic analysis of β-phosphoglucomutase and its inhibition by magnesium fluoride, *J. Am. Chem. Soc.*, 2009, **131**, 1575–1588.

13 N. J. Baxter, M. W. Bowler, T. Alizadeh, M. J. Cliff, A. M. Hounslow, B. Wu, D. B. Berkowitz, N. H. Williams, G. M. Blackburn and J. P. Waltho, Atomic details of near-transition state conformers for enzyme phosphoryl transfer revealed by MgF$_3^-$ rather than by phosphoranes, *Proc. Natl. Acad. Sci. U. S. A.*, 2010, **107**, 4555–4560.

14 B. Elsässer, S. Dohmeier-Fischer and G. Fels, Theoretical investigation of the enzymatic phosphoryl transfer of β-phosphoglucomutase: Revisiting both steps of the catalytic cycle, *J. Mol. Model.*, 2012, **18**, 3169–3179.

15 J. L. Griffin, M. W. Bowler, N. J. Baxter, K. N. Leigh, H. R. W. Dannatt, A. M. Hounslow, G. M. Blackburn, C. E. Webster, M. J. Cliff and J. P. Waltho, Near attack conformers dominate β-phosphoglucomutase complexes where geometry and charge distribution reflect those of substrate, *Proc. Natl. Acad. Sci. U. S. A.*, 2012, **109**, 6910–6915.

16 Y. Jin, D. Bhattasali, E. Pellegrini, S. M. Forget, N. J. Baxter, M. J. Cliff, M. W. Bowler, D. L. Jakeman, G. M. Blackburn and J. P. Waltho, α-Fluorophosphonates reveal how a phosphomutase conserves transition state conformation over hexose recognition in its two-step reaction, *Proc. Natl. Acad. Sci. U. S. A.*, 2014, **111**, 12384–12389.

17 J. Dai, L. Wang, K. N. Allen, P. Rådström and D. Dunaway-Mariano, Conformational cycling in β-phosphoglucomutase catalysis: Reorientation of the β-D-Glucose 1,6-(bis)phosphate intermediate, *Biochemistry*, 2006, **45**, 7818–7824.

18 L. Johnson, A. J. Robertson, N. J. Baxter, C. R. Trevitt, C. Bisson, Y. Jin, H. P. Wood, A. M. Hounslow, M. J. Cliff, G. M. Blackburn, M. W. Bowler and J. P. Waltho, van der Waals contact between nucleophile and transferring phosphorous is insufficient to achieve enzyme transition-state architecture, *ACS Catal.*, 2018, **8**, 8140–8153.

19 G. Zhang, J. Dai, L. Wang, D. Dunaway-Mariano, L. W. Tremblay and K. N. Allen, Catalytic cycling in β-phosphoglucomutase: A kinetic and structural analysis, *Biochemistry*, 2005, **44**, 9404–9416.

20 M. Monticelli, L. Liguori, M. Allocca, G. Andreotti and M. V. Cubellis, β-Glucose-1,6-bisphosphate stabilizes pathological phophomannomutase2 mutants *in vitro* and represents a lead compound to develop pharmacological chaperones for the most common disorder of glycosylation, PMM2-CDG, *Int. J. Mol. Sci.*, 2019, **20**, 4164.

21 P. S. Chan, C. T. Black and B. J. Williams, Separation of cyclic 3′,5′-AMP from ATPADP, and 5′-AMP by precipitation with inorganic compounds, *Anal. Biochem.*, 1973, **55**, 16–25.

22 M. Carlson, J. D. Carter and J. Rohloff, Improved preparation of 2 M triethylammonium bicarbonate, *Green Chem. Lett. Rev.*, 2015, **8**, 37–39.

23 H. P. Wood, F. A. Cruz-Navarrete, N. J. Baxter, C. R. Trevitt, A. J. Robertson, S. R. Dix, A. M. Hounslow, M. J. Cliff and J. P. Waltho, Allomorphy as a mechanism of post-transla-

tional control of enzyme activity, *Nat. Commun.*, 2020, **11**, 1–12.

24 N. J. Baxter, L. F. Olguin, M. Goličnik, G. Feng, A. M. Hounslow, W. Bermel, G. M. Blackburn, F. Hollfelder, J. P. Waltho and N. H. Williams, A Trojan horse transition state analogue generated by MgF_3^- formation in an enzyme active site, *Proc. Natl. Acad. Sci. U. S. A.*, 2006, **103**, 14732–14737.

25 F. Paradisi, J. L. Dean, K. F. Geoghegan and P. C. Engel, Spontaneous chemical reversion of an active site mutation: Deamidation of an asparagine residue replacing the catalytic aspartic acid of glutamate dehydrogenase, *Biochemistry*, 2005, **44**, 3636–3643.

26 L. E. Holt, J. A. Pierce and C. N. Kajdi, The solubility of the phosphates of strontium, barium, and magnesium and their relation to the problem of calcification, *J. Colloid Sci.*, 1954, **9**, 409–426.

27 J. E. Seegmiller and B. L. Horecker, The synthesis of glucose-6-phosphate and 6-phosphogluconate, *J. Biol. Chem.*, 1951, **192**, 175–180.

28 D. M. Brown and D. A. Usher, Hydrolysis of hydroxyalkyl phosphate esters: The epoxide route, *J. Chem. Soc.*, 1965, **1965**, 6547–6558.

29 D. M. Brown and D. A. Usher, Hydrolysis of hydroxyalkyl phosphate esters: Effect of changing ester group, *J. Chem. Soc.*, 1965, **1965**, 6558–6564.

30 M. A. C. Reed, A. M. Hounslow, K. H. Sze, I. G. Barsukov, L. L. P. Hosszu, A. R. Clarke, C. J. Craven and J. P. Waltho, Effects of domain dissection on the folding and stability of the 43 kDa protein PGK probed by NMR, *J. Mol. Biol.*, 2003, **330**, 1189–1201.

31 T. Posternak, Synthesis of α- and β-glucose-1,6-diphosphate, *J. Biol. Chem.*, 1949, **180**, 1269–1278.